JOURNAL OF CATALYSIS 64, 303–319 (1980)

# The Sintering of a Silica-Supported Nickel Catalyst

H. K. KUO, P. GANESAN, AND R. J. DE ANGELIS

*Department of Metallurgical Engineering and Materials Science, Institute for Mining and Minerals Research, University of Kentucky, Lexington, Kentucky 40506*

Received May 30, 1979; revised March 3, 1980

Changes in the average particle size and particle size distribution (PSD) were monitored during sintering of a silica-supported nickel catalyst. Sintering was carried out in nitrogen and hydrogen atmospheres from 500 to 800°C for times varying from 1 to 100 hr. The particle size distribution functions (PSDs) determined both by X-ray single profile analysis and transmission electron microscopy were in excellent agreement. The sintering process was found to occur very rapidly initially and then proceeded more slowly at longer times for temperatures higher than 600°C. The effects of sintering temperature on the changes of PSD were found to be more pronounced than the effects of sintering time. As sintering progresses, the PSDs developed long tails to the larger diameter side. Fitting the data to the sintering power-law gave exponent values of 13 and 14 for sintering below 700°C in nitrogen and hydrogen, respectively. Particle growth became much faster as sintering was carried out at 800°C in both atmospheres. The values of the sintering exponent change from 13 to 6 in nitrogen atmosphere and from 14 to 4 in hydrogen atmosphere. The large values of the sintering exponent and the changes in the PSDs obtained during sintering at temperatures of 700°C and below indicate that sintering occurs by a particle migration mechanism. However, the sintering results obtained at 800°C tend to indicate that the atomic migration mechanism is predominating.

## INTRODUCTION

Metal catalysts are generally employed in the form of small metal particles or crystallites dispersed on high-surface area supports. In this form a high ratio of metal atoms exists on the surface and an active catalyst results. The support also serves the function of physically separating the small metal particles, which tends to inhibit agglomeration of the small particles into larger ones. Strong interaction between the support and the metal particles also inhibits agglomeration. This agglomeration, known as sintering, occurs very rapidly in the unsupported metal catalysts and leads to fewer metal atoms at the surface of the support with consequent loss of catalyst activity. Sintering also occurs at high temperatures in supported metal catalysts and is the main source of catalyst thermal deactivation. The process of sintering, by definition, requires changes to occur in the particle size distribution (PSD) (*1*). The sintering behavior of a supported metal catalyst depends on the initial PSD and knowledge of the progressive changes in the PSD during sintering can assist in elucidating the mechanism of sintering in the supported metal catalysts. Therefore, a reliable determination of the initial PSD function and the changes occurring in the PSD during sintering becomes essential if the sintering process is to be understood and ultimately controlled.

Until recently, it was generally recognized that the use of X-ray diffraction in the study of catalysts was limited to the measurement of the average particle size using the breadth of a diffraction profile, either at half-maximum intensity or the integral half breadth. In a recent paper an X-ray diffraction method for determining the average particle size and the particle size distribution function of the supported metal catalysts was presented (*2*). The advantage of the technique developed is that only a single order of an X-ray profile is required. From the analysis of a single diffraction profile it was shown that it is possible to



0021-9517/80/080303-17$02.00/0

obtain the same structural parameters that result from the Warren (*3*) analysis of double-order X-ray profiles.

Other X-ray investigations on supported metal catalysts using either double-order analysis or single-order and the assumption of zero strain have been reported (*4–7*). However, in the single profile analysis technique reported recently (*2*), the microstrain contributions to line broadening are not assumed to be zero.

An obvious application of the X-ray diffraction technique is in following the changes in the PSD during sintering of supported metal catalysts. An initial investigation of this type concerned with sintering of coprecipitated nickel oxide on silica and alumina supports was reported by Ganesan *et al.* (*2*). In this study, it was observed that when the crystallite size was less than 20 Å and there existed a bimodal character to the particle size distribution function, the changes in the PSD during sintering indicated that sintering was occurring by the particle migration and coalescence mechanism (*8, 9*). When the average crystallite size in the material prior to sintering was greater than 20 Å, the changes in the PSD function observed during sintering indicated the operative sintering mechanism to be an atomic migration mechanism (*10*).

A natural extension of this early work was to perform a similar set of experiments on the same catalysts, as employed in the NiO study, after reduction to nickel metal. The purpose of this paper is to report the results of the investigation performed on a silica-supported nickel catalyst. A second objective is to provide correlations between X-ray measured PSDs and distribution functions of the same catalyst determined by transmission electron microscopy (TEM).

## EXPERIMENTAL

The silica-supported catalytic material (C150-1-01) used in this investigation, supplied by United Catalysts, Inc., Louisville, Kentucky, contains 51.7% Ni, 2.9% C, and 0.06% S. It has a surface area of 211 $m^2/g$, a pore volume of 0.34 $cm^3/g$, and a density of 1.05 $g/cm^3$. The catalytic material $NiO/SiO_2$ was produced by a coprecipitation process (*11*). This is one of the four catalytic materials reported in a previous investigation (*2*).

The as-received pellets of catalyst C150-1-01 were packed in a wire mesh and reduced at 500°C for 3 hr in flowing hydrogen. After reduction, samples were sintered in the reduction retort, at temperatures varying from 500 to 800°C for times varying from 1 to 100 hr in nitrogen and hydrogen atmospheres. The samples were then cooled to room temperature and passivated for 8 hr in a 0.2% $O_2$–$N_2$ mixture. X-Ray diffraction samples were prepared by grinding the pellets and pressing the powder at 7 MPa pressure to form a disc of 24 mm in diameter and about 3 mm thick. No heating of the specimens was observed during the processing to disc. The nickel(200) diffraction profile was recorded for all the conditions of sintering by step scanning ($\Delta 2\theta = \frac{1}{15}°$). The instrumental profile was employed to Stokes correct the Fourier coefficients obtained from the profiles of the catalyst specimens. The very low intensity of NiO(220) profile [less than 5% of the Ni(200) profile] indicated only a small amount of NiO was not reduced. The Ni(200) profiles were analyzed using the technique described previously (*2*) to obtain structural information including the particle size distribution functions (PSDs).

The values of the average particle size obtained from X-ray diffraction measurements made on the C150-1-01 catalyst in the "as-received" condition, following reduction at 500°C for 3 hr and after sintering at various times and temperatures under nitrogen and hydrogen atmospheres are reported in Tables 1 and 2. The average particle sizes of the same catalyst were measured by Park (*12*) using gas chemisorption techniques. There was excellent agreement among the data.

TABLE 1

Particle Sizes of Reduced Nickel Catalyst C150-1-101 during Sintering in Nitrogen Atmosphere

| Run number | Reduction | | Sintering | | | $D_{\text{half breadth}}$[a] (Å) | $D_{\text{one peak}}$[b] (Å) |
|---|---|---|---|---|---|---|---|
| | Temp. (°C) | Time (hr) | Temp. (°C) | Time (hr) | Atm. | | |
| As received (NiO) (Ref. 2) | | | | | | 28.8 | 20.4 |
| Average of numbers 17, 25, 32, 40 | 500 | 3 | — | — | — | 42.0 | 29.5 |
| 18 | 500 | 3 | 500 | 5 | $N_2$ | 43.4 | 30.6 |
| 19 | 500 | 3 | 500 | 10 | $N_2$ | 44.0 | 33.0 |
| 35 | 500 | 3 | 500 | 20 | $N_2$ | 45.5 | 35.3 |
| 20 | 500 | 3 | 500 | 50 | $N_2$ | 50.0 | 38.0 |
| 24 | 500 | 3 | 600 | 5 | $N_2$ | 48.0 | 33.0 |
| 26 | 500 | 3 | 600 | 10 | $N_2$ | 48.8 | 35.6 |
| 27 | 500 | 3 | 600 | 20 | $N_2$ | 49.0 | 37.7 |
| 21 | 500 | 3 | 600 | 50 | $N_2$ | 50.7 | 40.0 |
| 23 | 500 | 3 | 600 | 100 | $N_2$ | 51.5 | 41.2 |
| 77 | 500 | 3 | 700 | 5 | $N_2$ | 53.2 | 38.7 |
| 70 | 500 | 3 | 700 | 10 | $N_2$ | 64.7 | 41.1 |
| 31 | 500 | 3 | 700 | 20 | $N_2$ | 70.0 | 45.7 |
| 33 | 500 | 3 | 700 | 50 | $N_2$ | 77.0 | 48.4 |
| 34 | 500 | 3 | 700 | 100 | $N_2$ | 80.7 | 50.9 |
| 72 | 500 | 3 | 800 | 1 | $N_2$ | 67.4 | 45.6 |
| 73 | 500 | 3 | 800 | 5 | $N_2$ | 85.0 | 60.1 |
| 74 | 500 | 3 | 800 | 10 | $N_2$ | 98.0 | 67.1 |
| 75 | 500 | 3 | 800 | 20 | $N_2$ | 102.5 | 79.1 |
| 76 | 500 | 3 | 800 | 50 | $N_2$ | 125.4 | 96.6 |

[a] Effective particle size from half-intensity breadth of profile by Scherrer formula.
[b] Effective particle size from the single profile method of peak analysis.

The particle growth kinetics during sintering, according to Wynblatt and Gjostein (*13, 14*), can be expressed as:

$$n \log(R/R_0) = C + \log(t) \qquad (1)$$

where $C$ is a constant, $R$ is the average particle radius at time $t$, and $R_0$ is the initial particle radius. Plots of $\log(R/R_0)$ vs $\log(t)$ for data obtained by X-ray single profile analysis at different temperatures in nitrogen and hydrogen atmospheres are shown in Figs. 1 and 2. The slopes of the straight lines give the values of $n$ which yield the sintering order by the relationship $(n + 1)$. As can be seen, sintering at 500 and 600°C in nitrogen gave the $n$ value of 12 which corresponds to a sintering order value of 13. This large value of sintering order decreases slightly as the sintering temperature increases to 700°C. Sintering at 800°C in nitrogen, however, produces a significant decrease in the order of sintering to a value of 6. A similar change in the order of sintering has also been found during sintering in hydrogen atmosphere. As the temperature increases from 700 to 800°C, the order of sintering decreases from 14 to 4. These changes in the sintering order are believed to reflect a change in the sintering mechanism.

It should be pointed out here that the values of the sintering order obtained at temperatures of 700°C and below are greater than the maximum value predicted by the particle migration model (*8, 9*). According to the originally proposed particle

TABLE 2

Particle Sizes of Reduced Nickel Catalyst C150-1-01 during Sintering in Hydrogen Atmosphere

| Run number | Reduction | | Sintering | | | $D_{\text{half breadth}}$[a] (Å) | $D_{\text{one peak}}$[b] (Å) |
|---|---|---|---|---|---|---|---|
| | Temp. (°C) | Time (hr) | Temp. (°C) | Time (hr) | Atm. | | |
| 41 | 500 | 3 | 500 | 5 | $H_2$ | 47.8 | 33.6 |
| 42 | 500 | 3 | 500 | 10 | $H_2$ | 48.8 | 32.6 |
| 43 | 500 | 3 | 500 | 15 | $H_2$ | 48.8 | 32.0 |
| 44 | 500 | 3 | 500 | 20 | $H_2$ | 49.0 | 34.0 |
| 45 | 500 | 3 | 500 | 50 | $H_2$ | 50.0 | 38.8 |
| 47 | 500 | 3 | 600 | 5 | $H_2$ | 52.7 | 37.8 |
| 48 | 500 | 3 | 600 | 10 | $H_2$ | 54 | 39.0 |
| 49 | 500 | 3 | 600 | 15 | $H_2$ | 53.5 | 38.5 |
| 50 | 500 | 3 | 600 | 20 | $H_2$ | 55 | 41.6 |
| 51 | 500 | 3 | 600 | 50 | $H_2$ | 56.1 | 44.5 |
| 53 | 500 | 3 | 700 | 5 | $H_2$ | 61.1 | 45 |
| 54 | 500 | 3 | 700 | 10 | $H_2$ | 63.5 | 46.6 |
| 55 | 500 | 3 | 700 | 15 | $H_2$ | 70.3 | 47 |
| 56 | 500 | 3 | 700 | 20 | $H_2$ | 71.8 | 48.8 |
| 57 | 500 | 3 | 700 | 50 | $H_2$ | 73.4 | 52.5 |
| 66 | 500 | 3 | 800 | 1 | $H_2$ | 93.6 | 62.5 |
| 59 | 500 | 3 | 800 | 5 | $H_2$ | 129.7 | 69.0 |
| 60 | 500 | 3 | 800 | 10 | $H_2$ | 141.4 | 73.4 |
| 61 | 500 | 3 | 800 | 15 | $H_2$ | 178.3 | 82.4 |
| 62 | 500 | 3 | 800 | 20 | $H_2$ | 193.3 | 98.0 |

[a] Effective particle size from half-intensity breadth of profile by Scherer formula.
[b] Effective particle size from the single profile method of peak analysis.

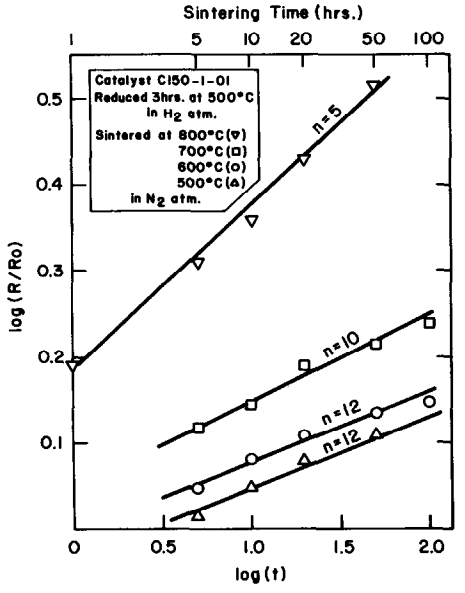


FIG. 1. Plot of $\log(R/R_0)$ vs $\log(t)$ for catalyst C150-1-01 sintered under a nitrogen atmosphere.

migration model, the value of the sintering order falls into the range between 2 and 8 depending upon the assumed rate determining step of the sintering process. However, as pointed out by Ruckenstein and Dadyburjor (*15*), sintering order with values larger than 8 can still be obtained if a diffusion controlled process with the diffusion coefficient inversely proportional to higher powers of the particle radius is assumed.

As shown in Table 2, sintering to hydrogen atmosphere results in a decrease in the average particle size for times less than 15 hr. A similar effect is also seen for the case of sintering at 600°C in hydrogen. This decrease in the average particle size during the initial stage of sintering in hydrogen is believed to be due to a further reduction. It was found on examining the NiO(220) diffraction profile for the as-reduced sample

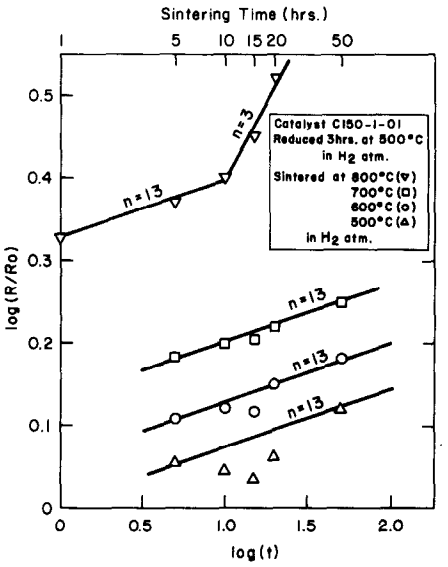


FIG. 2. Plot of $\log(R/R_0)$ vs $\log(t)$ for catalyst C150-1-01 sintered under a hydrogen atmosphere.

that a small amount of NiO remained in its unreduced form. In addition, from the chemisorption results (*12*) it was determined that reduction at 500°C for 3 hr did not reduce the catalyst completely. Therefore, during sintering in hydrogen, further reduction of the NiO particles which remained in the as-reduced sample occurs and leads to a decrease in the average particle size. Furthermore, it was found that sintering above 500°C in hydrogen always results in a larger value of average particle size as compared to the catalyst sintered in nitrogen. The effect of the sintering environment can be explained as due to the water which formed during the reduction process in hydrogen and aids in the transfer and growth of the metal particles (*16*). It is also believed that the NiO particles that would remain when sintering under nitrogen have a strong interaction with the support material and tend to hinder the particle growth process.

The PSDs obtained from four separate samples reduced at 500°C for 3 hr by hydrogen are shown in Fig. 3a. The very good agreement obtained for these four separate runs indicates the reproducibility of the data. A statistical analysis was performed on these four data sets, and the results are shown in Fig. 3b. The bars in this figure

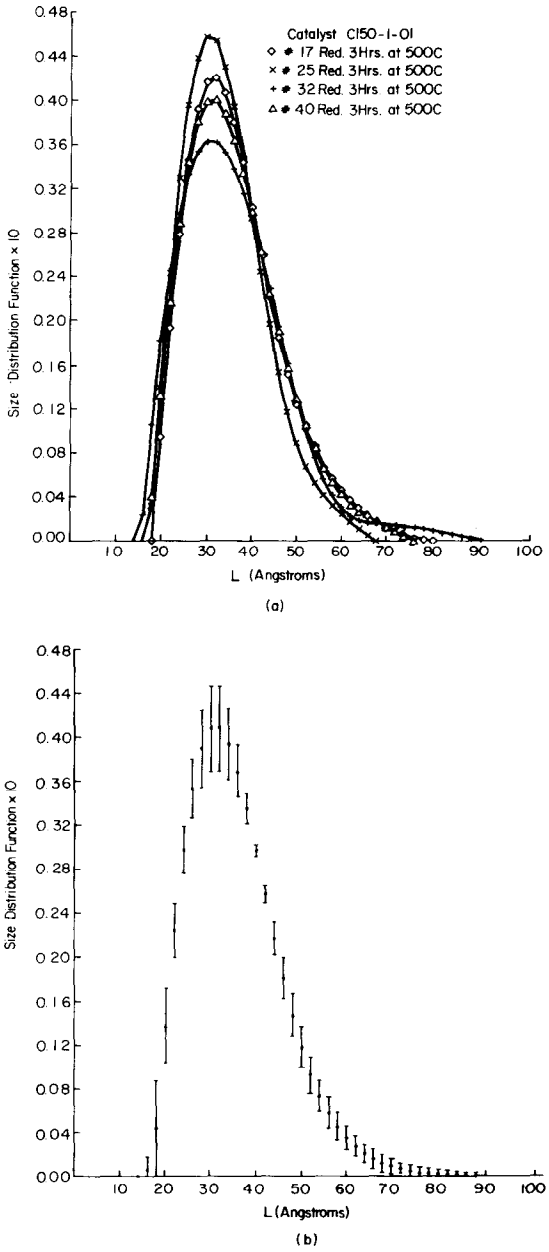


FIG. 3. (a) Particle size distribution functions from four separate samples of catalyst C150-1-01 reduced at 500°C for 3 hr. (b) Results of least square analysis of the four PSD data sets shown in (a). Bars indicate plus and minus one sigma variation about the average value of the PSD functions.

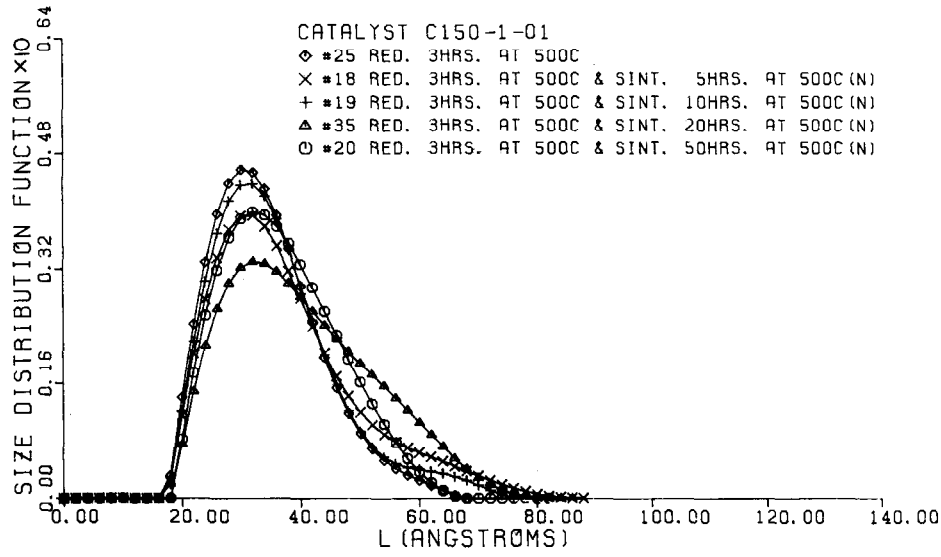


FIG. 4. Particle size distribution functions of catalyst C150-1-01 reduced at 500°C for 3 hr and sintered at 500°C for various times in nitrogen atmosphere.

indicate one standard deviation from the average values of the four PSD functions. From this figure it is also possible to determine the error in the intercepts of the PSD function with the abscissa. At the small crystallite size in the distribution the intercept range is 5 Å and at the large crystallite size the intercept range in 15 Å. This gives an indication of the reproducible nature of the reduction process and the analysis procedure. However, the experimental variations that arise during sintering do not reflect themselves in this data set.

A reduction at 500°C for 3 hr was employed on all samples prior to sintering. The PSDs obtained for samples reduced at

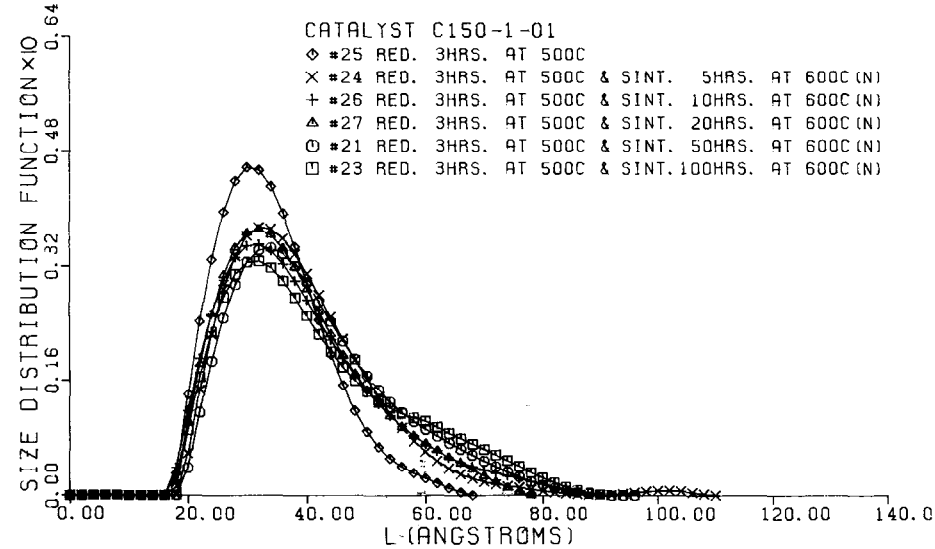


FIG. 5. Particle size distribution functions of catalyst C150-1-01 reduced at 500°C for 3 hr and sintered at 600°C for various times in nitrogen atmosphere.

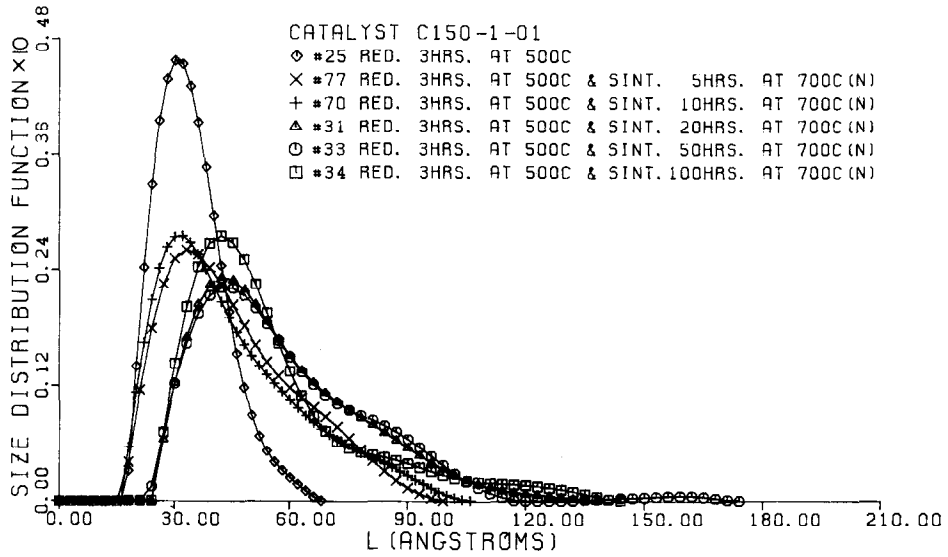


FIG. 6. Particle size distribution functions of catalyst C150-1-01 reduced at 500°C for 3 hr and sintered at 700°C for various times in nitrogen atmosphere.

500°C for 3 hr and sintered at 500, 600, 700, and 800°C for various times in nitrogen or hydrogen atmosphere are shown in Figs. 4–11. During sintering at 500°C the time of sintering has little effect on the PSD, only slight changes in the PSDs are detected in both the nitrogen and hydrogen atmospheres (Figs. 4 and 8). The PSD broadens during the initial stage of sintering at 600°C, however sintering for longer times does not change the PSD appreciably (Figs. 5 and 9). This is to say that the rate of sintering is relatively slow after an initial rapid change in the PSD function. This initial rapid change in the PSDs is also observed at 700 and 800°C sintering in both nitrogen and

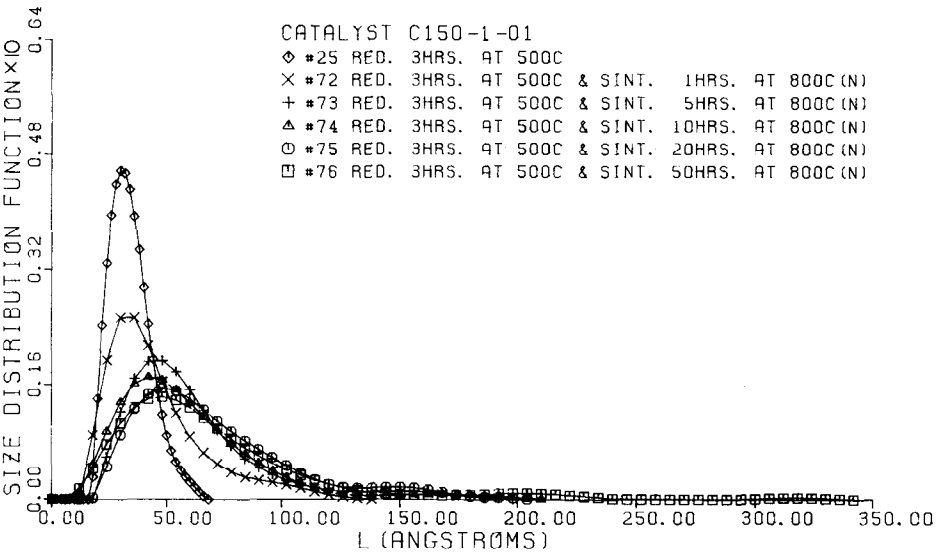


FIG. 7. Particle size distribution functions of catalyst C150-1-01 reduced at 500°C for 3 hr and sintered at 800°C for various times in nitrogen atmosphere.

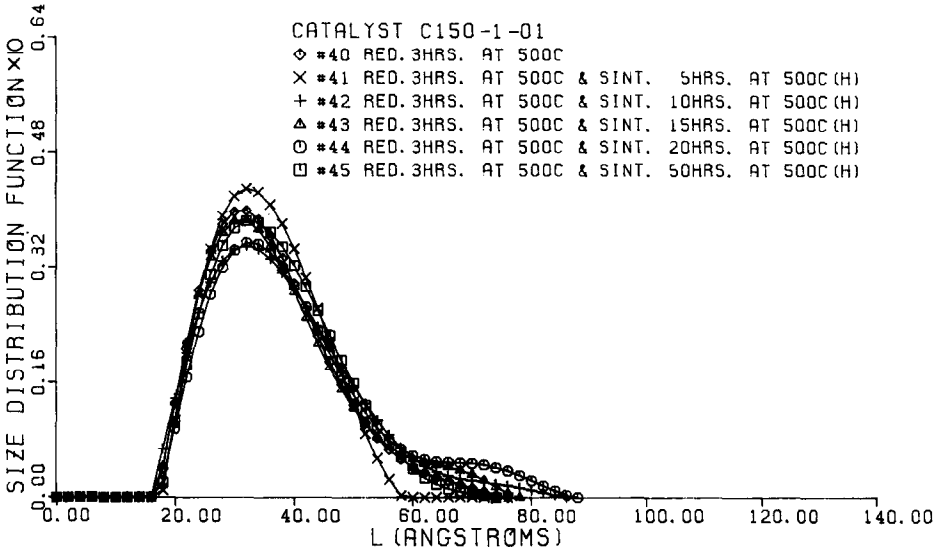


FIG. 8. Particle size distribution functions of catalyst C150-1-01 reduced at 500°C for 3 hr and sintered at 500°C for various times in hydrogen atmosphere.

hydrogen atmospheres (Figs. 6, 7, 10, and 11). During sintering at 600°C in nitrogen (Fig. 5) the large particle side of the distribution after sintering for 20 hr ends at a lower value than the PSD after sintering for 10 hr. This behavior can be explained by considering the possible variations in the samples which have been described in Figs. 3a and b.

The general trends of the changes in the PSDs during sintering at temperatures of 700°C and below are: the distributions broaden and form tails to the larger particle size side of the distribution functions.

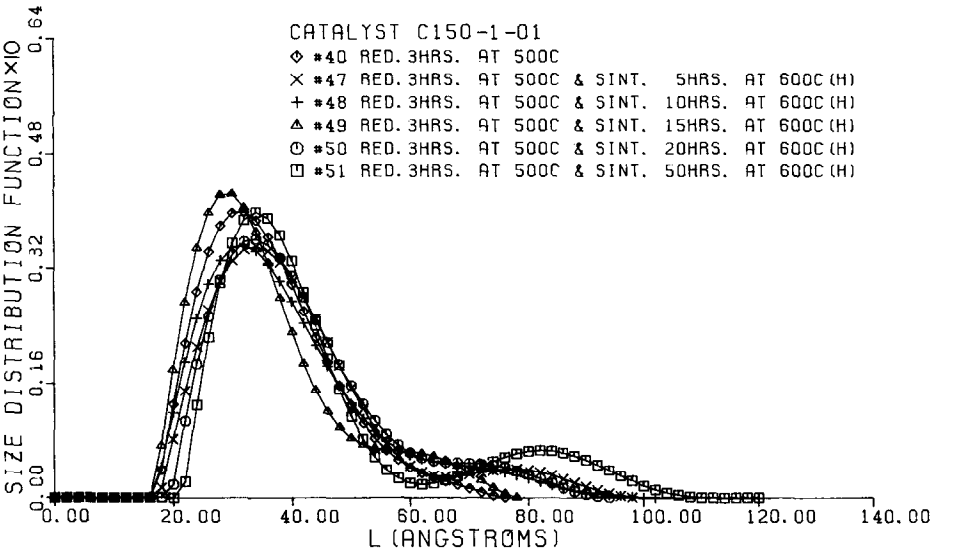


FIG. 9. Particle size distribution functions of catalyst C150-1-01 reduced at 500°C for 3 hr and sintered at 600°C for various times in hydrogen atmosphere.

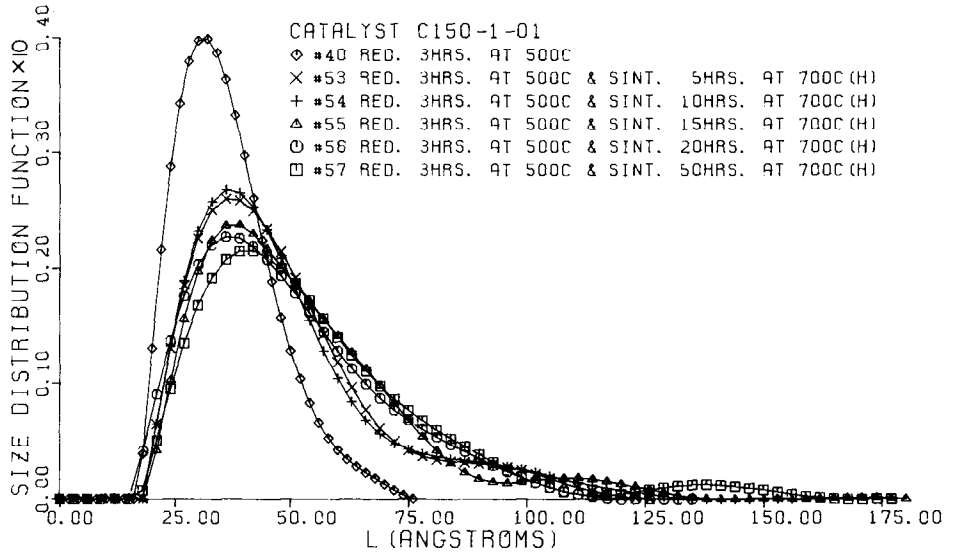


FIG. 10. Particle size distribution functions of catalyst C150-1-01 reduced at 500°C for 3 hr and sintered at 700°C for various times in hydrogen atmosphere.

There are indications that a slight bimodal character exists in a number of the distribution functions. In fact one of the PSDs shown in Fig. 3a has a slight bimodal character. Realizing that the four results in Fig. 3a were obtained from four different samples, it may indicate that the metal particles in some of the materials are distributed with a slight bimodal character. It is not possible to say if the bimodal functions observed during sintering developed during sintering or existed in the original sample selected for that run. To eliminate this uncertainty *in situ* reduction and sintering studies would

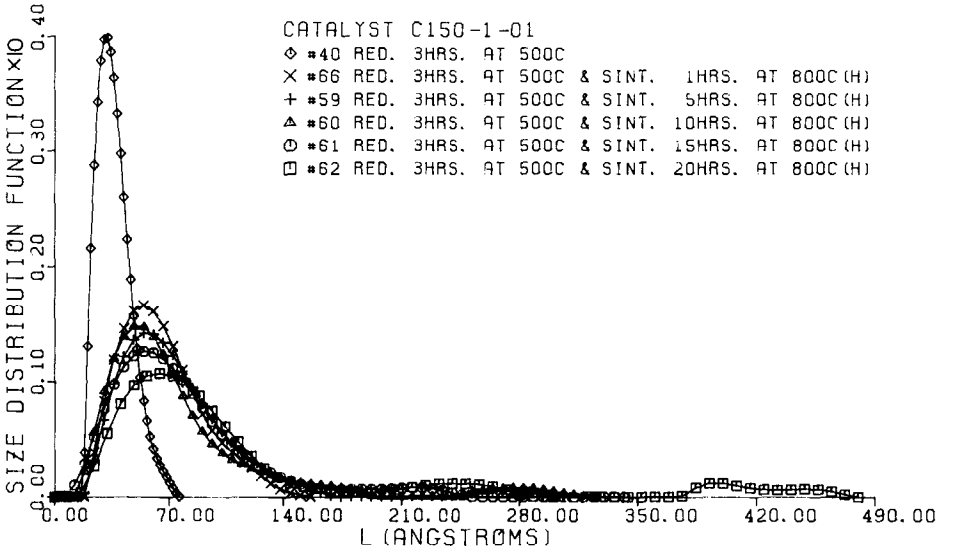


FIG. 11. Particle size distribution functions of catalyst C150-1-01 reduced at 500°C for 3 hr and sintered at 800°C for various times in hydrogen atmosphere.

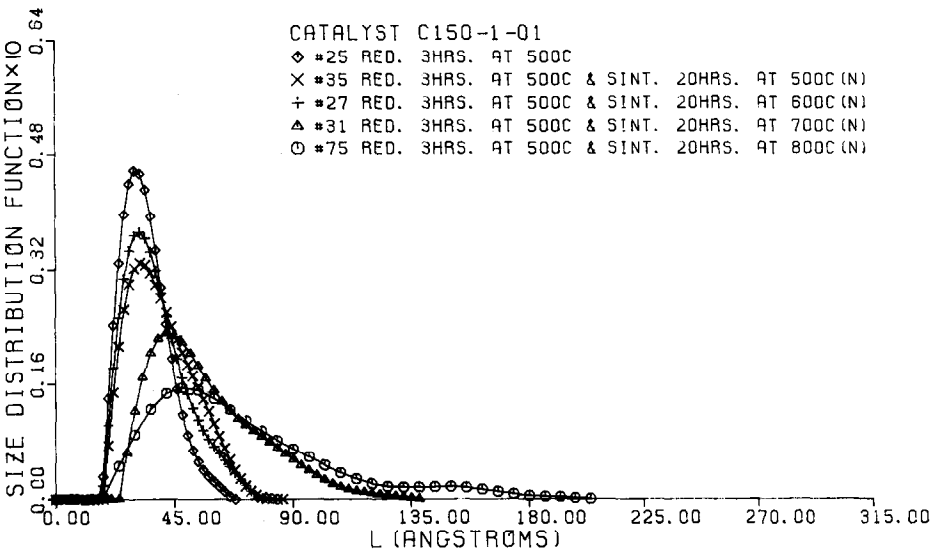


FIG. 12. Particle size distribution functions of catalyst C150-1-01 reduced at 500°C for 3 hr and sintered at 500, 600, 700, and 800°C for 20 hr in nitrogen atmosphere.

have to be performed on the X-ray unit allowing the same volume of material to be sampled by the beam in all conditions.

Sintering at 800°C under both nitrogen and hydrogen atmospheres produced particles which are smaller than the smallest particles existing in the as-reduced catalysts (see Figs. 7 and 11). This effect is interpreted as indicating that a different mechanism of sintering is in operation at 800°C than at the lower temperatures. It is likely that at 800°C which is a temperature greater than one-half of the nickel melting point that atomic mobility is high and that

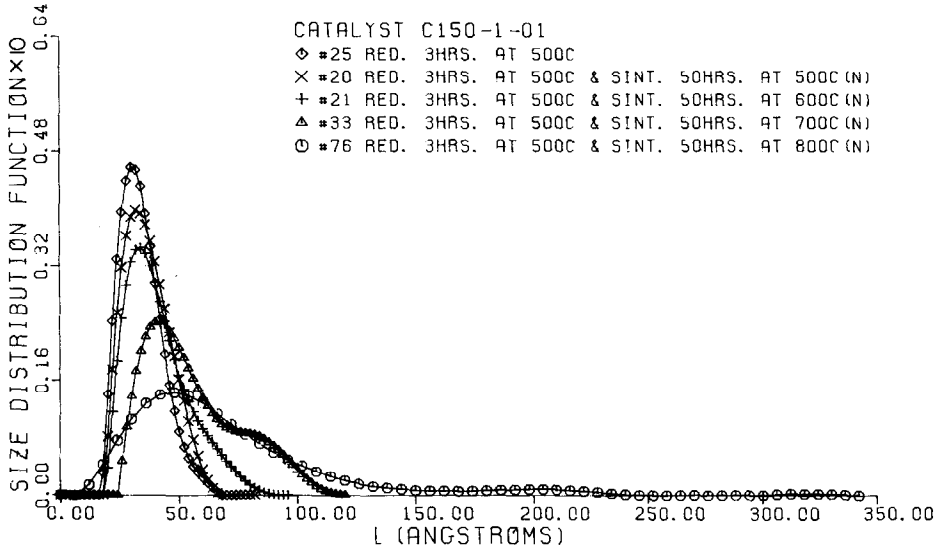


FIG. 13. Particle size distribution functions of catalyst C150-1-01 reduced at 500°C for 3 hr and sintered at 500, 600, 700, and 800°C for 50 hr in nitrogen atmosphere.

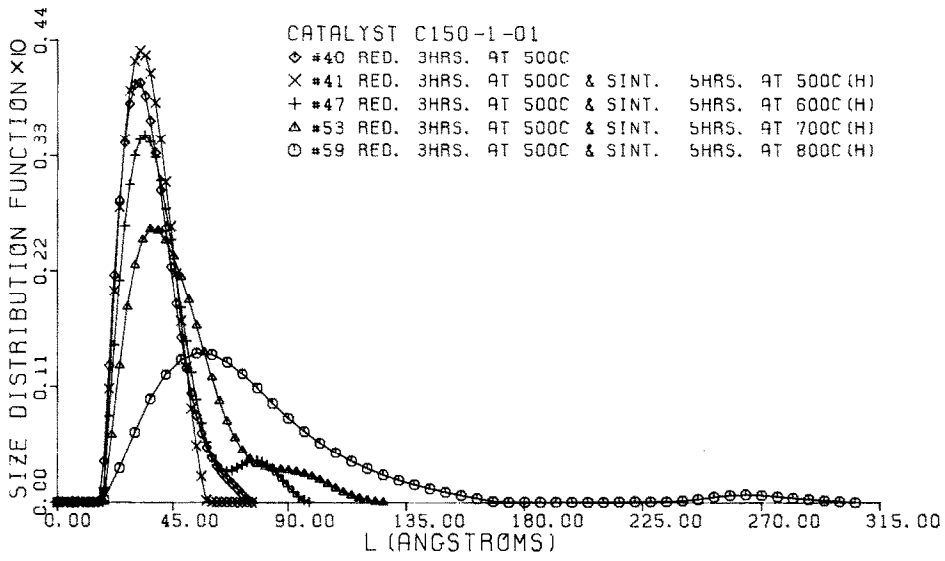


FIG. 14. Particle size distribution functions of catalyst C150-1-01 reduced at 500°C for 3 hr and sintered at 500, 600, 700, and 800°C for 5 hr in hydrogen atmosphere.

an atomic migration mechanism becomes the predominant mechanism for sintering process (*17*).

The isochronal behavior of PSDs during sintering of the catalyst C150-1-01 is shown in Figs. 12–15. As can be seen, the effects of sintering temperature on the PSD are much larger than the effects of sintering time. Increasing the sintering temperature always produces an increase in the number of particles in the larger size range of the distribution, especially at temperatures above 600°C. In addition to this, it is found that in most of the cases a small shift in the

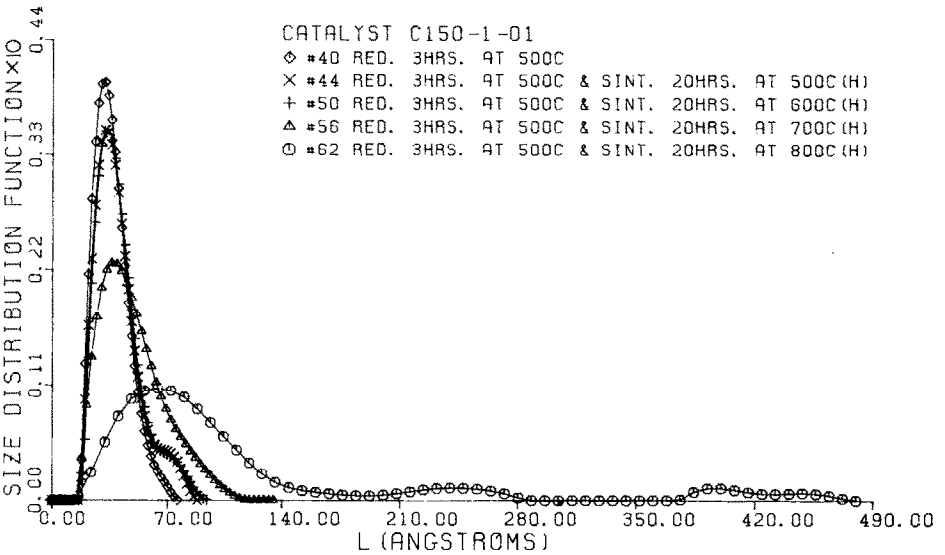


FIG. 15. Particle size distribution functions of catalyst C150-1-01 reduced at 500°C for 3 hr and sintered at 500, 600, 700, and 800°C for 20 hr in hydrogen atmosphere.

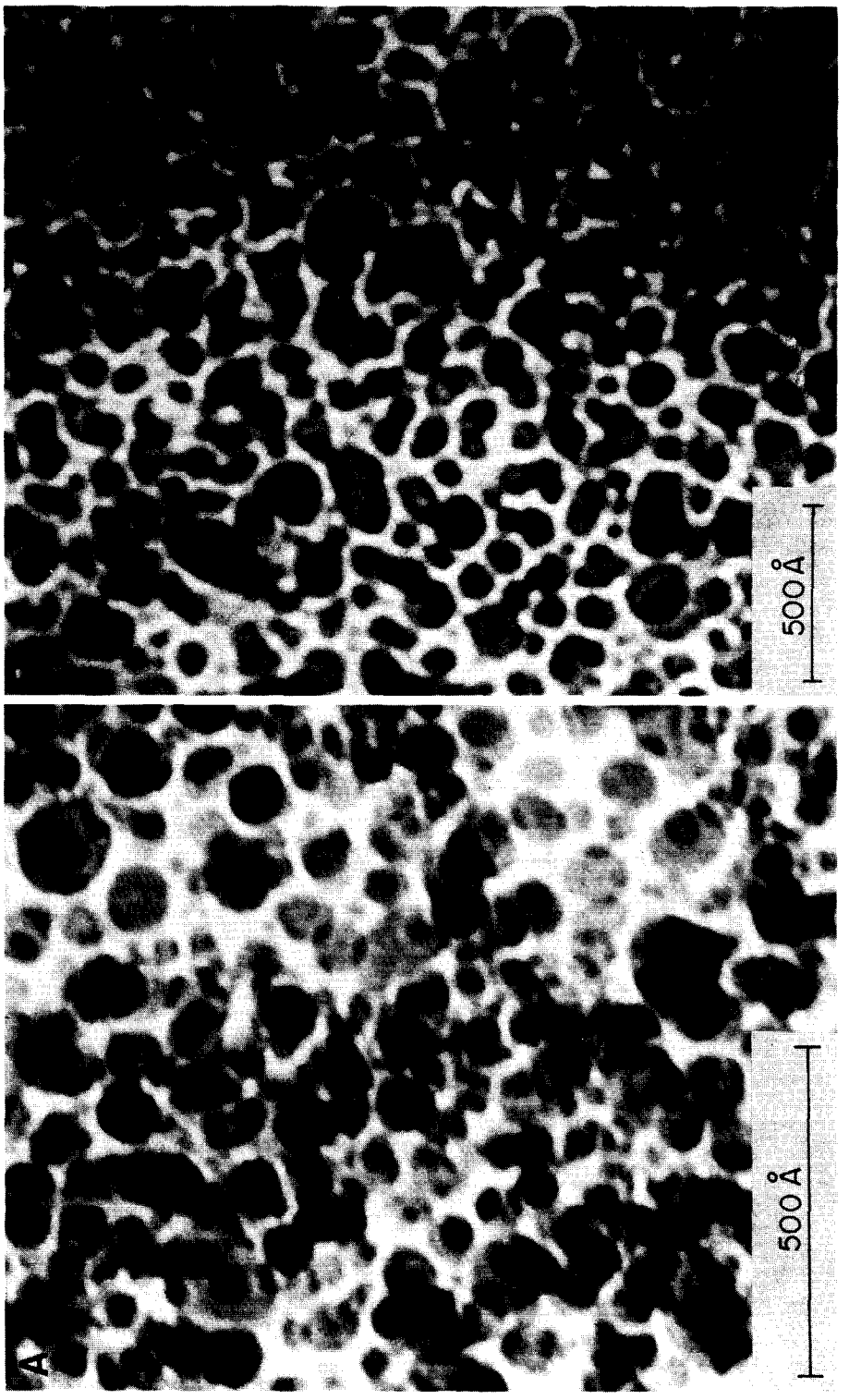
500 Å
500 Å
A

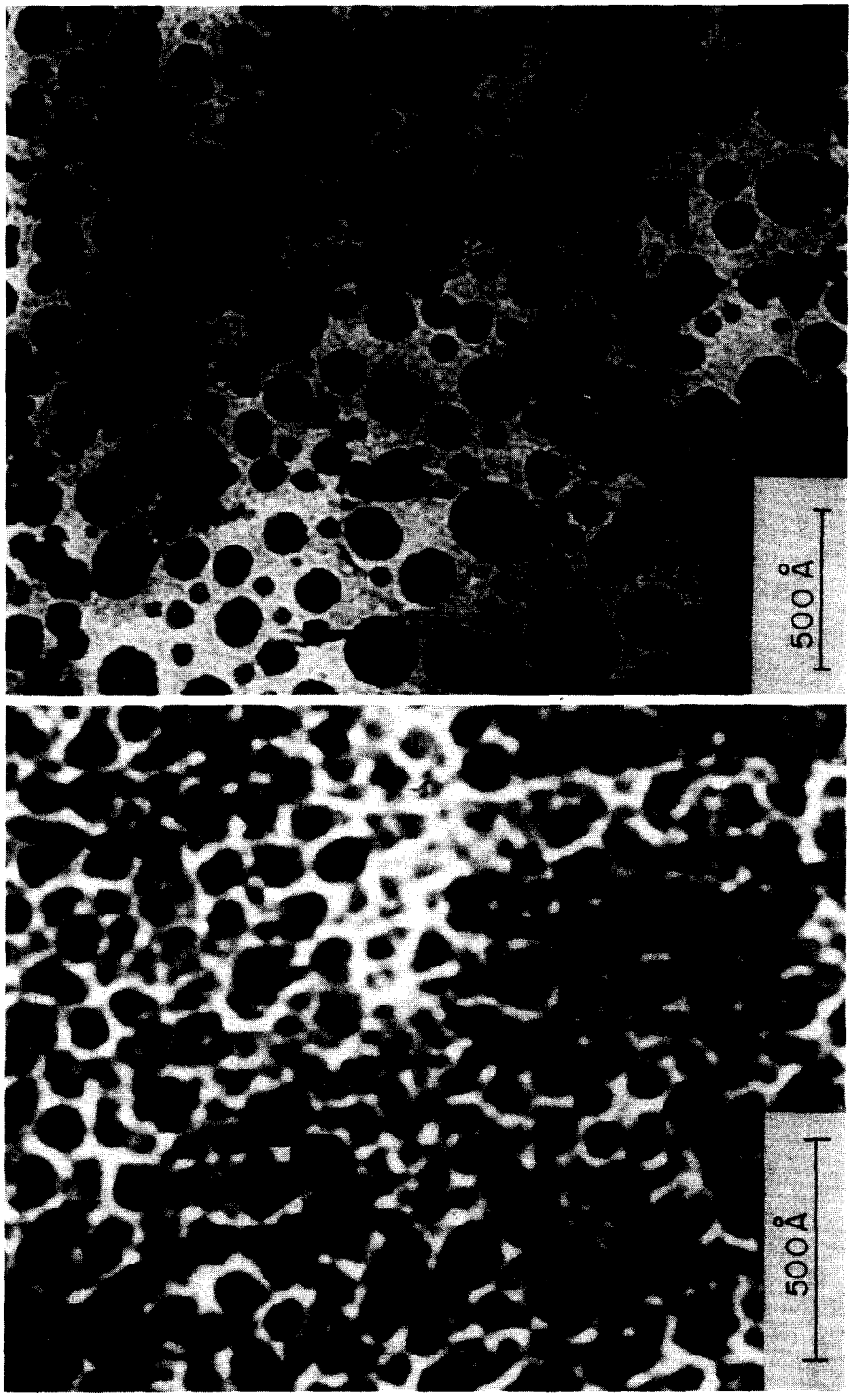


FIG. 16. Typical transmission electron micrographs of the silica-supported nickel catalyst C150-1-01; (a) as reduced (reduced at 500°C for 3 hr); reduced and sintered at: (b) 700°C for 100 hr in $N_2$, (c) 700°C for 50 hr in $H_2$, and (d) 800°C for 20 hr in $N_2$.

position of the maximum in the PSD to larger particle size when the sintering temperature was increased. This type of sintering behavior has also been reported by Renouprez *et al.* (*18*).

In order to check independently the validity of PSD functions determined by X-ray diffraction method, transmission electron microscopy work was done on specimens from five selected runs to obtain the PSDs by direct observation. TEM specimens were prepared by suspending the catalyst powder in methyl alcohol ultrasonically. A drop of the suspension solution was placed on a copper grid which was coated with carbon on Formvar and the alcohol was allowed to evaporate. After drying, the specimens were observed in a Hitachi HUll-B electron microscope set up for high-resolution observations. For each specimen photographs enlarged to greater than half a million magnification were produced. Tedious and time-consuming measurements of about 500 particles were made on each specimen to determine the PSD. Typical photographs of the "as-reduced" (reduced at 500°C for 3 hr) specimen and also specimens reduced and sintered at various conditions are shown in Fig. 16.

The resulting PSD functions, normalized to unit area, determined by TEM are shown in Figs. 17–21. Superimposed on the PSDs

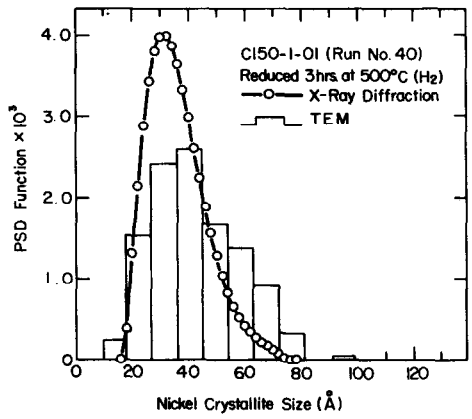


FIG. 17. Particle size distribution functions determined by TEM and X-ray diffraction for catalyst C150-1-01 in the as-reduced condition.

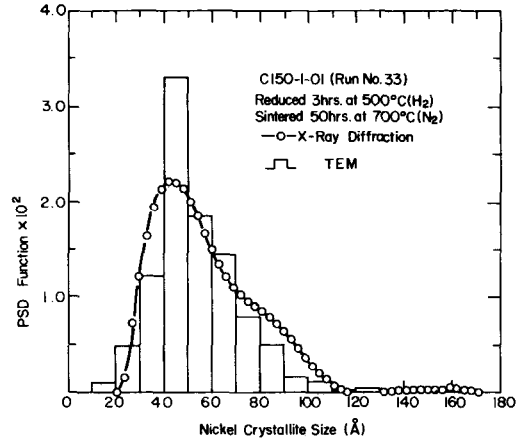


FIG. 18. Particle size distribution functions determined by TEM and X-ray diffraction for catalyst C150-1-01 reduced and sintered at 700°C for 50 hr in nitrogen atmosphere.

determined by TEM are the corresponding PSDs determined by the X-ray single profile analysis technique. The agreement between the results obtained from the two techniques is considered to be excellent, especially in the cases of the "as-reduced," sintered at 700°C for 50 hr in nitrogen and hydrogen atmosphere (Figs. 17–19). The agreement is not as good in the case of the specimen sintered at 700°C for 100 hr in nitrogen (Fig. 20). However, this specimen was stored in the atmosphere about 3 weeks after the X-ray work was completed and prior to making the TEM specimens. During this period of time a portion of the nickel metal possibly reoxidized, increasing the apparent sizes of the particles. However, if one considers the minute amount of the specimens used in the TEM work, the agreement observed in this case is still good.

Domain size distribution functions have been determined on $Cu_3Au$ using the Warren double-order X-ray technique and TEM (*19*) with similar agreement as obtained here. However, these are the initial comparison data to be reported which support the X-ray single profile analysis technique of determining the PSD functions. In addition, although PSDs determined by TEM

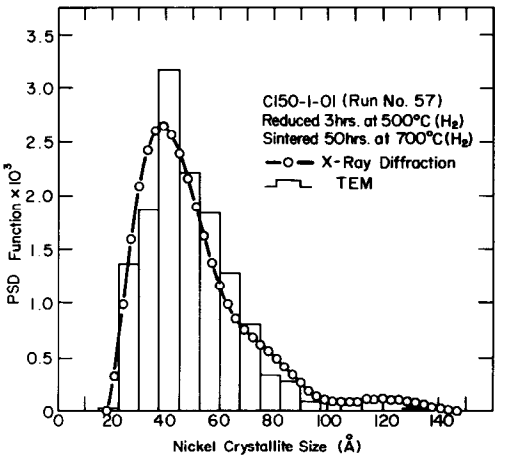


FIG. 19. Particle size distribution functions determined by TEM and X-ray diffraction for catalyst C150-1-01 reduced and sintered at 700°C for 50 hr in hydrogen atmosphere.

have been compared with the small angle X-ray results on a platinum catalyst (*18*), this is the first time X-ray line profile analysis and TEM determined PSD functions have been performed on a supported nickel catalyst.

## DISCUSSION

The results of this investigation make up a very complete set of PSD functions which describe the sintering behavior of a supported nickel catalyst. Because of the complete nature of the data its most significant value should be in providing insights into the operating mechanism of sintering. For this reason the discussion will be concerned with describing various aspects of the operative sintering mechanisms.

A number of characteristics of the sintering behavior have been observed here: the rapid rate of sintering at short sintering times, the development of an approximately stable particle size distribution at longer sintering times, the changes in the sintering order at 800°C, and the formation of smaller particles occurred only during sintering at 800°C. It is necessary to envoke two sintering mechanisms to account for all of these observations; one mechanism for temperatures of 700°C and below and another mechanism for 800°C. For lower temperatures, a particle migration model in which the maximum size of the migrating particles is proportional to the sintering temperature (*17*) is consistent with the data. Other observations which support this mechanism are the magnitude of the sintering order and the development of tails in the PSDs to the larger particle size side of the distribution.

During the initial stage of sintering, parti-

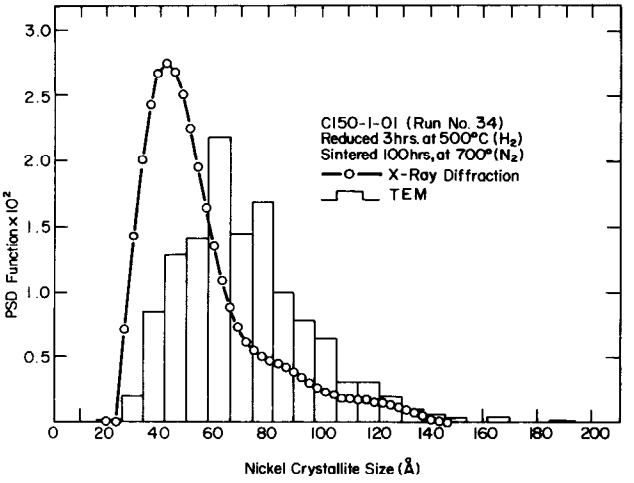


FIG. 20. Particle size distribution functions determined by TEM and X-ray diffraction for catalyst C150-1-01 reduced and sintered at 700°C for 100 hr in nitrogen atmosphere.

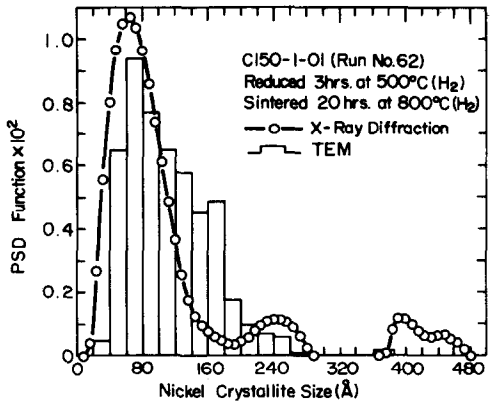


FIG. 21. Particle size distributrion functions determined by TEM and X-ray diffraction for catalyst C150-1-01 reduced and sintered at 800°C for 20 hr in hydrogen atmosphere.

cles smaller than the maximum mobile size migrate easily, collide, and coalesce with other particles to form larger particles. Energetically the favored positions for coalescence to occur would be in the concave portions of the pore structure (*20*). Migration of particles to concave regions in the pore structure has been suggested to be the process associated with initial rapid sintering rates (*20*). The migration process continues as long as migrating particles are available or until the growing particle fills the portion of the pore cavity in which it resides. At this point in the process the growth rate decreases substantially and the PSD function stabilizes. It is clear that considering sintering from this standpoint makes the topography and pore size distribution of the support primary characteristics which control the sintering behavior. A further indication of the influence of the support can be obtained from the sintering order data. The large values of the sintering order are attributed to a finite rate of coalescence which could be due to either a lack of migrating particles or a retardation of the migration process due to strong particle–support interaction.

Two sintering characteristics observed at 800°C are: the formation of particles smaller than those existing in the as-reduced material (see Figs. 7 and 11) and the decrease in sintering order (from 13 to 6 in $N_2$ and from 14 to 4 in $H_2$) which occurred during 800°C sintering (see Figs. 1 and 2). The sintering order (4 to 6) could be accounted for by both the atomic migration and particle migration models for sintering. However, considering that at 800°C smaller particles were observed to form during sintering, it is likely that the atomic migration mechanism is operating. Furthermore, unless one or more model parameters changes significantly it would not be possible for the particle migration mechanism to account for the changes in the sintering order observed at 800°C. For example, the diffusion coefficient or the rate constant of coalescence would have to vary suddenly and drastically. Variation such as these are not expected. Therefore, the changes in the sintering order are interpreted as indicating that the sintering mechanism changed from particle migration to atomic migration.

Considering the influence of the support, it would be expected that initially particles below a fairly large maximum particle size migrate, collide, and coalesce and fill pore sections very rapidly at 800°C. Once the pore sections, in which the coalesced particle resides, are filled the particle migration mechanism is suppressed. Further sintering required the operation of an atomic migration mechanism. When this occurs the sintering order would be expected to change and smaller particles would start decreasing their sizes. The smaller particles are the preferred particles for atoms to detach from and migrate to the larger particles existing in the pore structure.

In summary it has been suggested that the pore structure has primary control on the sintering behavior of a supported metal catalyst. At sintering temperatures of 700°C and below sintering occurs by a particle migration mechanism. When the number of migrating particles is exhausted or when the pore sections are filled, the rate of sintering decreases significantly. At 800°C sintering temperature, the pores are filled

rapidly by migrating particles and further sintering takes place by an atomic migration mechanism.

## CONCLUSION

(i) The average particle sizes and particle size distribution functions of a silica-supported nickel catalyst during sintering were determined by using X-ray diffraction and TEM methods. The excellent agreements of the PSDs from two methods indicate the recently developed single profile analysis technique to be reliable.

(ii) The effects of temperature on the sintering of silica-supported nickel catalyst are much more pronounced than the effects of the sintering time.

(iii) A stable PSD forms after the initial rapid sintering of the supported nickel catalyst and the PSD shifts to large values as the sintering temperature increases. The pore structure of the catalyst plays an important role in affecting the sintering behavior of the supported metal catalysts.

(iv) Sintering at temperatures of 700°C and below occurs by a particle migration mechanism. As the temperature increases to 800°C, sintering occurs by an atomic migration mechanism.

## ACKNOWLEDGMENT

This research was supported by the Energy Research and Development Agency through Contract No. EX-76-C-01-2229.

## REFERENCES

1. Wanke, S. E., and Flynn, P. C., *Catal. Rev.* **12,** 93 (1975).
2. Ganesan, P., Kuo, H. K., Saavedra, A., and De Angelis, R. J., *J. Catal.* **52,** 310 (1978).
3. Warren, B. E., *Prog. Metal Phys.* **8,** 152 (1959).
4. Pausescu, P., Manaila, R., and Popescu, M., *J. Appl. Crystallogr.* **7,** 281 (1974).
5. Shephard, F. E., *J. Catal.* **14,** 148 (1969).
6. Coenen, J. W. E., and Linsen, B. G., *in* "Physical and Chemical Aspects of Adsorbents and Catalysis," (B. G. Linsen, Ed.), p. 471. Academic Press, London, 1970.
7. Sashital, S. R., Cohen, J. B., Burwell, R. L., Jr., and Butt, J. B., *J. Catal.* **50,** 479 (1977).
8. Ruckenstein, E., and Pulvermacher, B., *AIChE J.* **19,** 356 (1973).
9. Ruckenstein, E., and Pulvermacher, B., *J. Catal.* **29,** 224 (1973).
10. Flynn, P. C., and Wanke, S. E., *J. Catal.* **34,** 390, 400 (1974).
11. Shalvoy, R. B., and Reucroft, P. J., *J. Catal.* **56,** 336 (1979).
12. Park, J. W., Master of Science Thesis, University of Kentucky, 1979.
13. Wynblatt, P., and Gjostein, N. A., *Scripta Met.* **9,** 969 (1973).
14. Wynblatt, P., and Gjostein, N. A., *Prog. Solid State Chem.* **9,** 21 (1975).
15. Ruckenstein, E., and Dadyburjor, D. B., *J. Catal.* **48,** 73 (1977).
16. Bartholomew, C. H., and Farrauto, R. J., *J. Catal.* **45,** 41 (1976).
17. Baker, R. T. K., *Catal. Rev.-Sci. Eng.* **19,** 161 (1979).
18. Renouprez, A., Hoang-Van, C., and Compagnon, P. A., *J. Catal.* **34,** 411 (1974).
19. Sakai, M., and Mikkola, D. E., *Met. Trans.* **2,** 1635 (1971).
20. Wynblatt, P., and Ahn, T.-M., *in* "Materials Science Research," (G. C. Kuczynski, Ed.), Vol. 10, p. 83. Plenum Press, New York, and London, 1975.